

Radar scatterometer observations of sastrugi on the great ice sheets

David G. Long, Ivan S. Ashcraft and Jeremy B. Luke

Brigham Young University, 459 Clyde Building, Provo, UT 84602, USA

ABSTRACT

The SeaWinds instrument on the QuikSCAT satellite was designed to measure near surface winds over the ocean; however, this remarkable remote sensing instrument has proven very useful in polar ice studies. Unlike previous radar scatterometers which were limited to 2 or 3 azimuth angles, the Ku-band SeaWinds instrument uses a circular scanning pencil beam, allowing it to make radar backscatter measurements from all azimuth angles. This geometry makes it an ideal candidate for studies of azimuth modulation of the normalized radar cross section of natural surfaces. Previous studies have observed a second order azimuth modulation of radar backscatter on the Antarctic ice sheet, which has been related to wind-generated sastrugi (snow dunes) on the surface. In this paper we use SeaWinds data to make more detailed studies of the azimuth modulation in both Antarctica and Greenland where little has been done.

Using the higher azimuth resolution possible with SeaWinds, we find that the azimuth variation of the backscatter is better described using a fourth order model in areas with the highest modulation. The orientation of these fourth order terms appears to be highly correlated to the katabatic wind direction. Azimuth modulation is also observed over Greenland, but it is much smaller than over Antarctica. Comparing SeaWinds and ERS-1/2 scatterometer mode data we examine the frequency dependence, finding the modulation larger at C-band than Ku-band. The largest azimuth modulation in Greenland is observed in the transition region between dry snow and percolation zones.

Keywords: scatterometer, SeaWinds, radar backscatter, ocean winds, QuikSCAT, radar equation

1. INTRODUCTION

While originally designed for ocean wind observation, scatterometer data have proven remarkably useful in a variety of cryosphere studies. Over large regions of Antarctica, wind-generated snow dunes with scales varying from a few meters to hundreds of kilometers influence the microwave backscattering of the surface, combining to introduce azimuth-angle dependencies in scatterometer data. Prior studies^{1,2} have demonstrated that scatterometer data can be used to infer the katabatic wind direction over Antarctica.

Previous fan-beam scatterometers such as ERS-1/2 and the NASA Scatterometer (NSCAT), provide only very limited azimuth angle sampling due to their antenna geometries. This has hampered further investigations into the azimuth dependence of the microwave scattering from snow and firn. The pencil-beam SeaWinds scatterometer, which has been flying on QuikSCAT since 1999, provides much greater diversity in azimuth than does previous instruments, particularly when multiple orbits are combined. We exploit this essential characteristic of the SeaWinds data to study the azimuthal dependence of backscatter over the great ice sheets of Antarctica and Greenland. In this paper we first provide some brief background on radar scatterometry, consider a simple descriptive model for the azimuth modulation of the backscatter over firn, and then evaluate the azimuth modulation over Antarctica and Greenland. Finally, we provide a brief discussion and summary.

Further author information: (Send correspondence to DGL)

DGL: E-mail: long@ee.byu.edu, Telephone: 1 801 422 4383

ISA: E-mail: ashcraft@ee.byu.edu, Telephone: 1 801 422 4884

JBL: E-mail: luke@ee.byu.edu

Table 1. Selected Antarctic study areas.

Area Number	Lower-Left Corner		Upper-Right Corner	
	lon	lat	lon	lat
1	88	-73	92	-74
3	135	-73	140	-74
7	87	-70.5	90	-71.5

2. SCATTEROMETRY BACKGROUND

Wind scatterometers are designed to measure the normalized radar cross section (σ°) of the Earth's surface. The near-surface wind over the ocean is inferred with the aid of a geophysical model function.³ To do this, scatterometers make measurements of the same patch of the surface from multiple azimuth angles as the satellite passes overhead. Due to the orbital and antenna geometries, previous fan-beam scatterometers (NSCAT and ERS-1/2) could make azimuth observations at no more than 6-8 essentially discrete azimuth angles (see Long and Drinkwater¹). SeaWinds, however, is the first of an entirely new class of wind scatterometer. Rather than collecting data over a range of incidence angles using fixed fan-beam antennas at different azimuth angles, SeaWinds uses a dual-beam, conically rotating antenna. It collects data at two fixed incidence angles, but over a wide range of azimuth angles. SeaWinds employs a contiguous, 1800 km wide observation swath,⁴ while NSCAT employs two 600 km swaths separated by a nadir gap.³ ERS-1/2 operates at C-band, has a single 500 km wide swath, and uses only a single polarization.⁵ Both SeaWinds and NSCAT are dual-pol and operate at Ku-band.

Scatterometers have proven very useful in the study of land surfaces and polar ice, see.⁶ Scatterometer data have been used to measure snow accumulation in Greenland⁷ and winds over Antarctic firn.^{1,2} The latter application is based on measuring the wind-induced surface roughness, which causes an azimuthal dependence of the radar backscatter.

For firn and snow Long and Drinkwater¹ proposed a second order descriptive model for the variation of σ° with azimuth angle. (They also incorporated an incidence angle dependence in their model, though this is not applicable to the SeaWinds case.) Their model describes the variation of σ° in terms of a Fourier series in azimuth angle, ϕ ,

$$\sigma^\circ(dB) = I_0 + \sum_{k=1}^N M_k \cos(k\phi + \psi_k) \quad (1)$$

where $N = 2$. Based on the limited azimuth angles available from the NSCAT and ERS-1/2 sensors, this model is appropriate. However, the better azimuth sampling of SeaWinds enables us to unambiguously evaluate if higher N values should be used to model the variation. As noted later, over Antarctica, we find that $N = 4$ often fits better than $N = 2$, suggesting that more sophisticated models for the structure of sastrugi are required than have previously been proposed, at least for some regions.

3. ANTARCTICA

Over the Antarctic ice sheet radiative cooling of surface air masses causes negative buoyancy and, as a result, the air sinks downslope. Ice sheet topography controls the drainage of these airmasses, funneling them into narrow areas on their way to the sea. Antarctic ice sheet surface winds maintain nearly the same speed and direction for weeks at a time, making them the most persistent winds on Earth.⁸ As a result, sastrugi and snow drifts form aligned with the wind direction. Their roughness is regionally dependent upon both the shape of the ice sheet directing the flow and variability in the magnitude of the wind vector. Such erosional and depositional features are believed to be the dominant source of the previously observed azimuth variation in σ° .¹ Because of this persistence in the wind we can assume that the azimuth modulation is stable over a several day period, permitting us to combine multiple passes in this analysis.

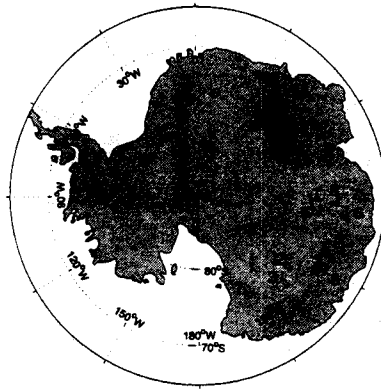


Figure 1. Locations of study regions.

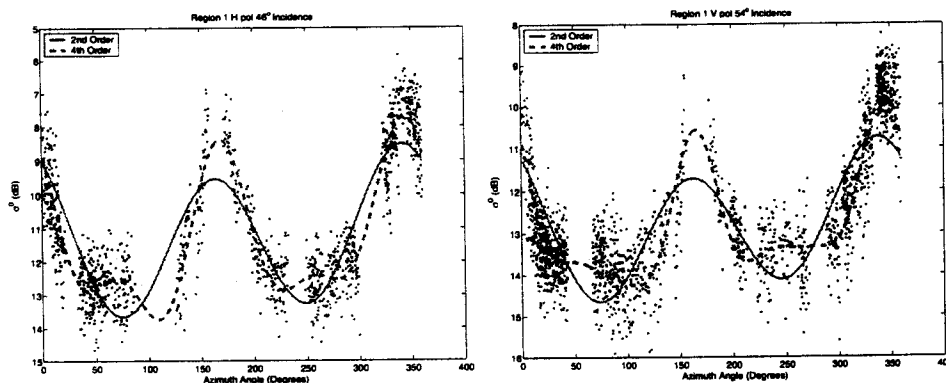


Figure 2. σ° vs azimuth angle for Region 1 showing both raw σ° measurements and 2nd and 4th order model fits to the data. (left) H-pol. (right) V-pol. There is clear evidence of a fourth order modulation.

We use SeaWinds data to examine the microwave response as a function of azimuth angle for a number of Antarctic study regions (see Fig. 1). These were selected in a manner similar to the study regions of Long and Drinkwater¹ and span a variety of surface characteristics. We consider three regions here (see Table 1). Note that the precise range of azimuth angles available at any given point depend on the details of the swath and orbital geometries and varies with latitude and polarization. Near the pole, the range of azimuth angles sampled diminishes.

Figures 2-4 illustrate the results of fitting the azimuth model given in Eq. 1 for $N = 2$ and $N = 4$ over several of the study regions. Each polarization is considered separately and only regions with adequate azimuth angle are considered. Inspection of the σ° versus azimuth angle plots in these figures clearly reveals that while much of the variation is described by the second order terms, fourth order terms are required to accurately describe the full variation of σ° with azimuth angle for regions 1 (Fig. 2) and 7 (Fig. 4). The smaller variation in σ° with azimuth seen in region 3 (Fig. 3) can be adequately described by a second order model. These observations apply to both polarizations. It is interesting to note that in regions 1 and 7 the peaks in the azimuth response are much sharper and the minima much wider than in region 3. These features are captured in the fourth order model fit.

Further evidence of the importance of the fourth order model over Antarctica comes from continent-wide images of the observation model parameters generated from SeaWinds measurements (see Fig. 5). Unfortunately, the observation geometry near the poles precludes accurate estimation of the model parameters here. This is seen as noisy magnitude estimates in the area surrounding the pole. Elsewhere, however, significant

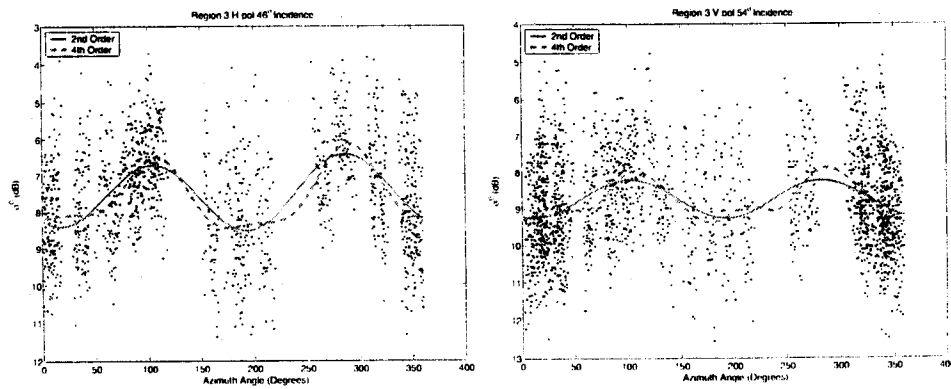


Figure 3. σ^0 vs azimuth angle for Region 3 showing both raw σ^0 measurements and 2nd and 4th order model fits to the data. (left) H-pol. (right) V-pol. The evidence for a fourth order modulation term is much less clear.

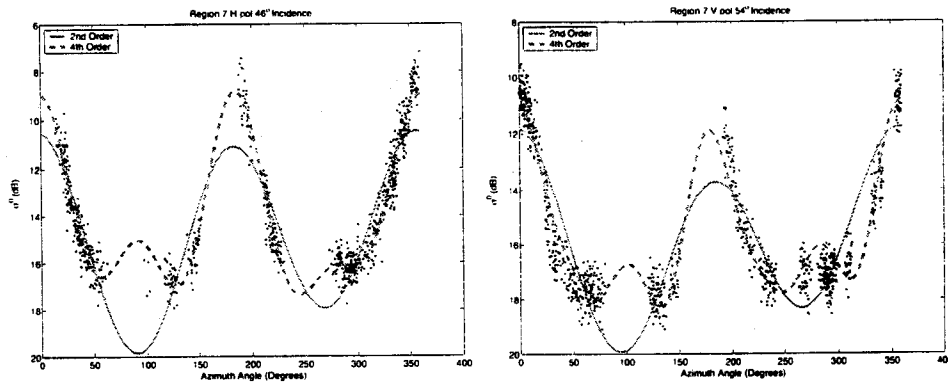


Figure 4. σ^0 vs azimuth angle for Region 7 showing both raw σ^0 measurements and 2nd and 4th order model fits to the data. (left) H-pol. (right) V-pol. A fourth order modulation model more accurately fits the data.

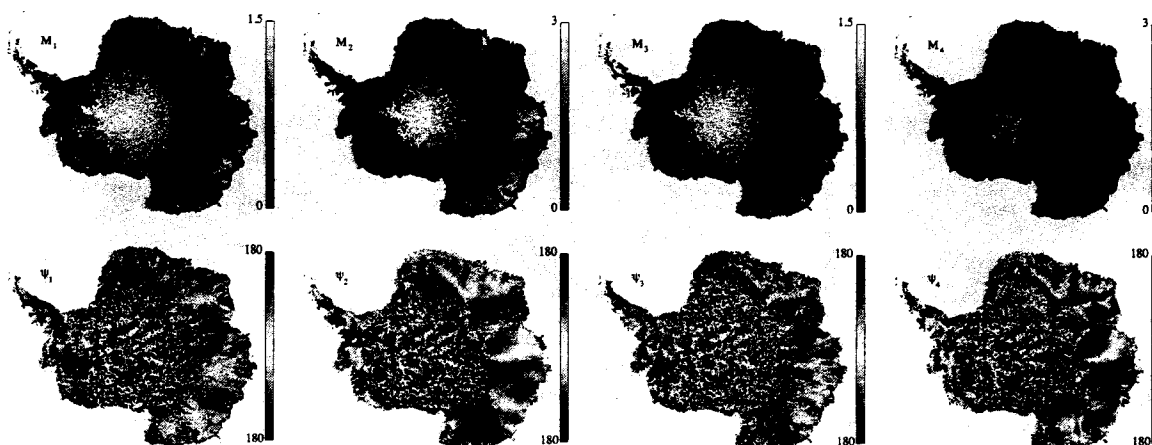


Figure 5. Fourth order azimuth observation model parameters (Eq. 1) estimated from SeaWinds on QuikSCAT data. The upper row contains images of the Fourier series magnitudes while the lower row contains images of the phase of the Fourier series terms. The azimuth sampling in the central region about the pole generally does not permit accurately estimating the fourth order observation model parameters. Spatial consistency is revealed in the large regions of similar parameter values. The second and fourth order phases are closely correlated with the local topographic slope.

spatial consistency can be seen in both the magnitudes and phases of the Fourier series terms. In particular, large areas of the lower right quadrant show significant modulation and spatially homogeneous phase. While the first and third order magnitudes are relatively small, the second and fourth order terms are much larger. We note that the second order phase term has been previously related to the katabatic wind direction and icesheet topography.¹ The fourth order term is largest near the coast (particularly in the lower right quadrant where particularly high speed katabatic winds are observed) and is also related to the wind direction and local topography. Virtually all the terms exhibit significant spatial consistency of magnitude phase in these coastal regions. Observations made over an annual cycle show little temporal variations in these patterns.

To validate the observation model, the standard deviation of the residual difference between the model fit and the raw σ° measurements is computed in Fig. 6. There are several contributions to this deviation, including the inherent variability of the measurements due to noise (which establishes a minimum standard deviation level), azimuth dependence, and spatial variability of the surface over each individual resolution element of the imaging grid. In Fig. 6 small scale features are generally the result of spatial variability of the 50 km grid used to compute the model parameters. As the model order is increased from $N = 0$ (azimuth modulation ignored) to $N = 4$, the residual error decreases. The noise variability can account for a large fraction of the residual error in the fourth order model plot, suggesting that a fourth order model adequately describes the observed variability.

4. GREENLAND

Over Greenland katabatic winds also play a dominant role in wind patterns with mean wind speeds over 10 m/s.⁹ Such winds, though less persistent than their Antarctic counterparts, sculpt the snow surface forming features which result in anisotropies in the backscatter measurements. Our object in including Greenland data in this study is to examine the σ° measurements for the presence of azimuth modulation and to investigate the frequency dependence of the azimuth modulation.

4.1. Observed modulation

Two locations on the Greenland ice sheet are considered in this analysis (see Fig. 7). Study areas are selected based on the relatively high modulation observed within them by QuikSCAT. As noted in Ref.¹⁰ the regions exhibiting the highest azimuth modulation for Ku-band measurements are along the transition region between

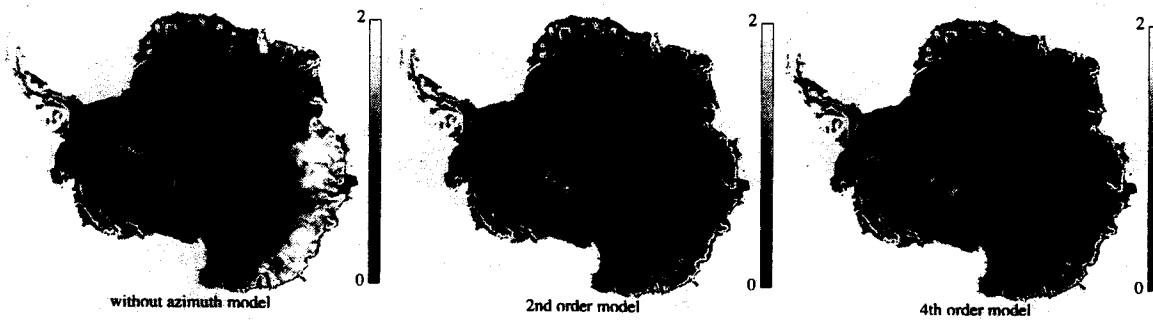


Figure 6. Standard deviation of the residual modeling error for the cases (left) no azimuth model ($N = 0$), (center) second order azimuth model ($N = 2$), and (right) fourth order azimuth model ($N = 4$). The finest detail is associated with sharp transitions in the surface backscatter and is due primarily to the resulting spatial inhomogeneity over the instrument footprint – in effect, an imaging artifact.

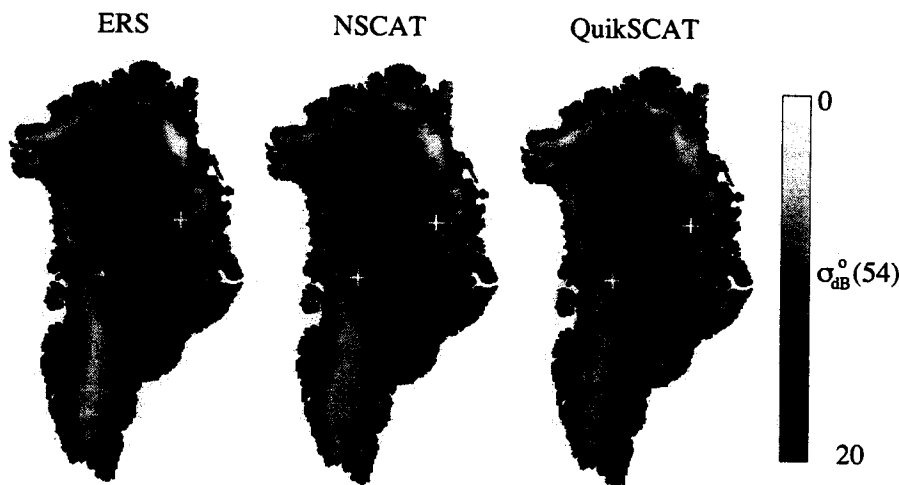


Figure 7. Backscatter images (σ° in dB at 54° incidence angle) of Greenland. The study locations are indicated on each image with location 1 at 74.4° N, 30.0° W and location 2 at 71.6° N, 45.8° W.

the dry snow and percolation facies. Thus both locations are in this region, one on the west of the ice sheet and one on the east.

The data employed in this analysis originates from three sensors: QuikSCAT, ERS-2, and NSCAT. Each of the sensors uniquely contributes to an improved understanding the processes driving the azimuth modulation. ERS operates at 5.3 GHz and spans a wide range of incidence angles, but only a limited number of azimuth directions. NSCAT operates at 13.6 GHz with a dual sided swath and a different antenna geometry, resulting in better azimuth sampling. SeaWinds offers nearly a continuous range of azimuth samples but at only a single incidence angle for each polarization. We inter-compare the data from all of these sensors to better understand the azimuth modulation. ERS and NSCAT are used to establish the combined incidence and azimuth dependence while SeaWinds is used to determine the finer details of the modulation at a single incidence angle. Because ERS measurements are only at v-pol and NSCAT h-pol measurements have insufficient azimuth sampling, only v-pol data is considered in this analysis.

The ERS and NSCAT data sets span 31 days while only three days of QuikSCAT are considered. This is in part due to the dense sampling and wide swath width of the SeaWinds instrument on QuikSCAT. All of the data is from the month of October with ERS and NSCAT data spanning JD 270 through 300, 1996, and SeaWinds data spanning JD 270 through 272, 2001. All data within a 30 km radius of each location and

Table 2. Observation model parameters at Greenland study location 1.

	<i>A</i>	<i>B</i>	<i>M</i> ₁	<i>M</i> ₂	<i>φ</i> ₁	<i>φ</i> ₂
ERS	-12.9	-0.25	0.73	1.72	147	38
NSCAT	-8.90	-0.19	0.22	0.60	7	27
QuikSCAT	-8.84	-	0.22	0.51	172	42

Table 3. Observation model parameters at Greenland study location 2.

	<i>A</i>	<i>B</i>	<i>M</i> ₁	<i>M</i> ₂	<i>φ</i> ₁	<i>φ</i> ₂
ERS	-19.4	-0.16	0.88	1.07	-2	113
NSCAT	-13.8	-0.22	0.46	0.31	-16	26
QuikSCAT	-11.4	-	0.43	0.45	-19	24

within an incidence angle (θ) range constrained to $40^\circ < \theta < 60^\circ$ are included. The incidence angle data filter is employed to ensure that the ERS and NSCAT data are compatible with the v-pol QuikSCAT data which is limited to 54° incidence angle.

To account for the incidence angle dependence, an additional term is added to the model in Eq. 1 for ERS and NSCAT,

$$\sigma^\circ(\text{dB}) = A + B(\theta - \theta_{ref}) + \sum_{k=1}^N M_k \cos(k\phi + \psi_k) \quad (2)$$

where θ is the incidence angle and $\theta_{ref} = 54^\circ$. The incidence angle dependence of the M_i terms¹ is negligible in the study regions at the given incidence angle range and thus is not included in the analysis. The azimuth anisotropies observed in the Greenland data are illustrated in the plots in Fig. 8. The azimuth dependence of the data for all the sensors is described well by the second order fit. No fourth order modulation is observed in the QuikSCAT data. We note that the maximum azimuth modulation in the SeaWinds data is much smaller (~ 1 dB versus ~ 8 dB) in the Greenland data than in the Antarctic data.

The orientation of the azimuth modulation is similar between the three sensors. The location of the minima in the backscatter are of particular interest because in Antarctica these minima correspond to the up/down wind direction.² At location 1 the katabatic wind is predominantly from the west,⁹ consistent with the minimum observed near 270° in the data. At location 2 a south-east wind dominates⁹ consistent with the minimum near 110° .

Although similar, there are some distinct differences between the C- and Ku-band modulations. At location 2 the modulation at C-band appears to be shifted by almost 50° relative to Ku-band. In Tables 2 and 3 the azimuth modulation is much larger at C-band than Ku-band, with the M_i terms two to three times larger at C-band than Ku-band. This is consistent with the results in Ref.¹⁰ The magnitude of the azimuth modulation observed by NSCAT and SeaWinds are nearly equal despite the five year time difference. The mean σ° (A) values are over 4 dB lower at C-Band than at Ku-band, while the B values (which aid in distinguishing between surface and volume scattering) do not seem to depend on the band: at location 2, where the backscatter is lowest, the incidence angle dependence is larger at Ku-band than at C-band; at location 1 it is larger at C-band.

4.2. Discussion

The clear difference between the azimuth modulation observed by C- and Ku-band can be explained by multiple surface attributes. First, recall that $\sigma^\circ(54^\circ)$ is much smaller at C-band than at Ku-band. For ERS, the wavelength $\lambda = 5.66$ cm, while for NSCAT and QuikSCAT, $\lambda \approx 2.2$ cm. Assuming the volume scattering component is primarily Mie scattering, the volume backscatter is proportional to r^6/λ^4 . Thus, the bulk volume scattering difference between C- and Ku-band is reduced by approximately 16 dB. However, the observed difference is only 4 dB, suggesting that surface scattering must play a significant role in the difference. At

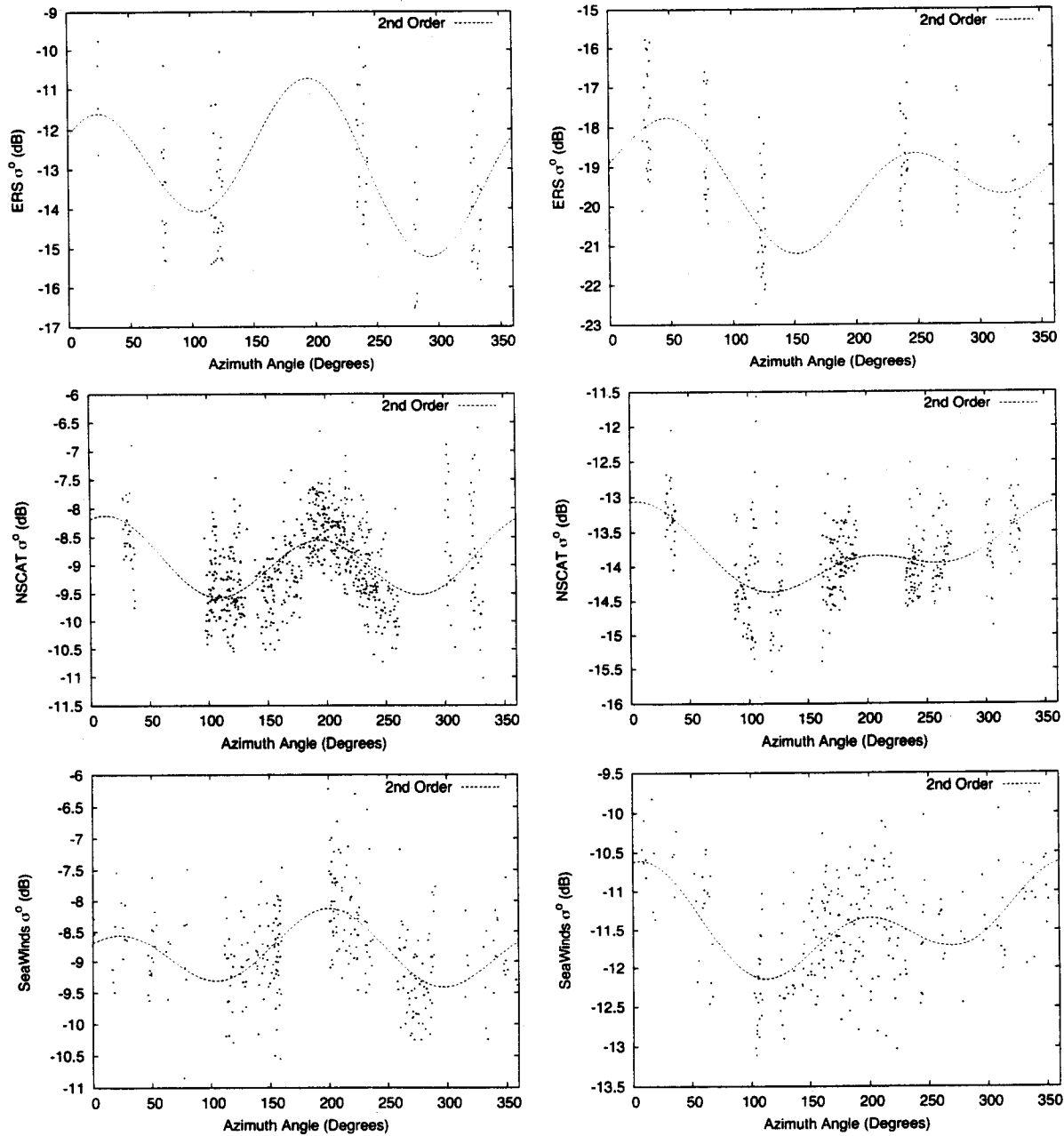


Figure 8. Scatter plots of the azimuth modulation observed over Greenland. The plots on the left are from location 1 and the plots on the right are from location 2 (see Fig. 7).

ERS C-band, the volume scattering is expected to play a smaller role than at Ku-band. We thus conclude that surface scattering at Ku-band is crucial for understanding the azimuth modulation. One caveat with this explanation is that over areas where surface scattering plays a dominant role the incidence angle dependence of the backscatter is expected to be larger. However as previously noted, the B values (which describe the incidence angle dependence) are larger at C-band than Ku-band at location 1, but not at location 2. Further analysis is required to understand this dichotomy.

5. SUMMARY

Significant modulation of σ° with azimuth angle occurs in both Antarctica and Greenland, though Greenland exhibits smaller modulation. Additional insight is available by comparing observations at C- and Ku-band. From our analysis, it appears that azimuth modulation must exceed a threshold before a fourth order modulation model is required to accurately describe it. Greenland does not reach above that threshold because the azimuth modulation is relatively small. However, over a significant portion of Antarctica, the fourth order modulation is clearly observed. Applying the simple surface model from Ref.,¹⁰ sharp peaks and deep, wide valleys in the azimuth modulation occur, similar to those found in the fourth order model. However, over Greenland, the same model yields a response similar to the second order azimuth dependence model. These observations lend credence to the model.

ACKNOWLEDGMENTS

This work was funded as part of the Ocean Vector Winds Science Team. SeaWinds data was obtained from the Physical Oceanography Distributed Data Archive (PO.DAAC) at the CalTech Jet Propulsion Laboratory.

REFERENCES

1. D. Long and M. Drinkwater, "Azimuth variation in microwave scatterometer and radiometer data over Antarctica," *IEEE Trans. Geosci. Remote Sens.* **38**(4), pp. 1857–1870, 2000.
2. M. Ledroit, F. Remy, and J. F. Minster, "Observations of the Antarctica ice sheet with the Seasat scatterometer: relation to katabatic-wind intensity and direction," *Journal of Glaciology* **39**(132), pp. 385–396, 1993.
3. F. Naderi, M. Freilich, and D. Long, "Spaceborne radar measurement of wind velocity over the ocean—an overview of the NSCAT scatterometer system," *Proc. IEEE* **79**(6), pp. 850–866, 1991.
4. M. Spencer, C. Wu, and D. Long, "Improved resolution backscatter measurements with the SeaWinds pencil-beam scatterometer," *IEEE Trans. Geosci. Remote Sens.* **38**(1), pp. 89–104, 2000.
5. E. Attema, "The active microwave instrument onboard the ERS-1 satellite," *Proc. IEEE* (6), pp. 791–799, 1991.
6. D. Long, M. Drinkwater, B. Holt, S. Saatchi, and C. Bertoia, "Global ice and land climate studies using scatterometer image data," *EOS, Trans. American Geophysical Union* **82**(43), p. 503, 23 Oct. 2001.
7. M. Drinkwater, D. Long, and A. Bingham, "Greenland snow accumulation estimates from scatterometer data," *J. Geophysical Res.* **106**(D24), pp. 33935–33950, 2001.
8. T. Parish and D. Bromwich, "The surface windfield over the Antarctic ice sheet," *Nature* **328**, pp. 51–54, 1987.
9. D. H. Bromwich, Y. Du, and K. M. Hines, "Wintertime surface winds over the Greenland ice sheet," *Monthly Weather Review* **124**, pp. 1941–1947, September 1996.
10. I. S. Ashcraft and D. G. Long, "Relating microwave backscatter azimuth modulation to surface properties of the Greenland Ice Sheet," in *IEEE International Geoscience and Remote Sensing Symposium*, 2003.